DOI: 10.1002/ejic.200600138

Bonding Trends in Lewis Acid Adducts of S_4N_4 – X-ray Structure of $TeCl_4 \cdot S_4N_4$

Jari Konu,[a] Tom Bajorek,[a] Risto S. Laitinen,*[a] Tristram Chivers,[b] Reijo J. Suontamo,[c] and Markku Ahlgrén[d]

Keywords: Lewis acid adducts of S_4N_4 / Tellurium tetrachloride / DFT calculations / Vibrational spectroscopy / X-ray crystallography

Tetrasulfur tetranitride and tellurium tetrachloride react in dichloromethane to form a 1:1 adduct $TeCl_4 \cdot S_4N_4$ (**1**). The crystal structure of **1** shows that $TeCl_4$ is bonded to the S_4N_4 ring through a Te–N linkage. As a consequence, the transannular S···S bonds in S_4N_4 are broken and the molecule assumes an open, monocyclic conformation. The Te–N bond of 2.16(1) Å is slightly longer than the single bond. The S–N bonds span a range of 1.55(1)–1.67(1) Å. The adduct **1** was also characterized by mass spectrometry and Raman spectroscopy. The bonding and spectroscopic properties of **1** are compared by DFT calculations at the B3PW91/(RLC ECP) level of theory with those of $BF_3 \cdot S_4N_4$ (**2**), $SO_3 \cdot S_4N_4$ (**3**), $AsF_5 \cdot S_4N_4$ (**4**), $SbCl_5 \cdot S_4N_4$ (**5**) for which experimental structural information is available. The structural and bonding trends in $TeF_4 \cdot S_4N_4$ (**6**), $TeBr_4 \cdot S_4N_4$ (**7**), and $SeX_4 \cdot S_4N_4$ [X = F (**8**), Cl (**9**), Br (**10**)] are also discussed.

Introduction

Tetrasulfur tetranitride is known to react in inert solvents with a wide variety of Lewis acids and a number of 1:1 adducts have been structurally characterized. The crystal structures are known for $BF_3 \cdot S_4N_4$,[1] $SO_3 \cdot S_4N_4$,[2] $AsF_5 \cdot S_4N_4$,[3] $SbCl_5 \cdot S_4N_4$,[4–6] $FeCl_3 \cdot S_4N_4$,[7,8] $TaCl_5 \cdot S_4N_4$,[9] and $TiCl_4 \cdot S_4N_4$.[10] The complexes $SnCl_4 \cdot 2S_4N_4$[11] and $TiCl_4 \cdot 2S_4N_4$[10] exemplify structurally characterized adducts with a 1:2 stoichiometry. However, the number of other known tellurium tetrahalide adducts containing a Te–N bond is sparse. Gieren et al.[12] have reported the crystal structure of $TeF_4(NNCHCHCH)_2$ and Massa et al.[13] have determined that of $[Te_6N_8(TeCl_4)_4] \cdot 4THF$.

The preparation of $TeCl_4 \cdot S_4N_4$ (**1**) by the reactions of S_4N_4 with $TeCl_4$ in various solvents,[14–16] or $S(NSO)_2$ with $TeCl_4$ in CH_2Cl_2[17] has been reported. The compound, however, was identified only by elemental analysis and IR spectroscopy. While Paul et al.[14] concluded on the basis of conductance measurements that in the solid state **1** has an ionic structure, Alange et al.[15] inferred $TeCl_4 \cdot S_4N_4$ to be a covalent coordination complex by comparing the IR spectrum of the adduct with those of the structurally characterized analogues $BF_3 \cdot S_4N_4$ and $SbCl_5 \cdot S_4N_4$. Ginn et al.[16] used **1** to produce a platinum complex containing the ^{15}N-labelled $TeSN_2$ ligand, but they did not provide structural details of $TeCl_4 \cdot S_4N_4$.

In this paper, we describe the structural and vibrational characterization of **1** and demonstrate that the compound represents one further example of a tellurium tetrahalide bonded to nitrogen. DFT MO calculations have been utilized to compare the trends in the molecular structures, bonding, stabilities, and spectroscopic properties of **1**, $BF_3 \cdot S_4N_4$ (**2**), $SO_3 \cdot S_4N_4$ (**3**), $AsF_5 \cdot S_4N_4$ (**4**), and $SbCl_5 \cdot S_4N_4$ (**5**) for which there is experimental information available, and to evaluate the corresponding properties in $TeF_4 \cdot S_4N_4$ (**6**), $TeBr_4 \cdot S_4N_4$ (**7**), and $SeX_4 \cdot S_4N_4$ [X = F (**8**), Cl (**9**), Br (**10**)]. $S_4N_4H^+$ (**11**) is included in this study for comparison.[18]

Results and Discussion

Synthesis and Spectroscopic Characterization of $TeCl_4 \cdot S_4N_4$ (1)

$TeCl_4 \cdot S_4N_4$ was produced by the reaction of S_4N_4 with $TeCl_4$ in CH_2Cl_2 as orange powder in ca. 76% yield. The EI mass spectrum of the product shows $TeS_4N_4^+$ (m/z = 314) as the fragment with highest mass. Although the mass spectrum shows no evidence of the molecular ion, the fragmentation pattern indicates the correct composition for $TeCl_4 \cdot S_4N_4$. The observed and calculated isotopic distributions were in good agreement for all fragments.

The ^{14}N NMR spectrum of the reaction solution from which the orange precipitate was removed by filtration

[a] Department of Chemistry, University of Oulu, P. O. Box 3000, 90014 Oulu, Finland
Fax: +358-8-553-1608
E-mail: risto.laitinen@oulu.fi
[b] Department of Chemistry, University of Calgary, Calgary, Alberta T2N 1N4, Canada
[c] Department of Chemistry, University of Jyväskylä, P. O. Box 35, 40014 Jyväskylä, Finland
[d] Department of Chemistry, University of Joensuu, P. O. Box 111, 80101 Joensuu, Finland
Supporting information for this article is available on the WWW under http://www.eurjic.org or from the author.

shows one resonance at δ = –256 ppm, but we did not observe the ^{125}Te resonance. The single resonance in the ^{14}N NMR spectrum is assigned to S_4N_4.[20] The compound **1** is expected to give rise to one resonance in the ^{125}Te NMR spectrum and three resonances with the intensity ratio of 1:2:1 in the ^{14}N NMR spectrum. Conductance measurements[14] imply that **1** has a different structure in solution than that observed in the solid state. The NMR spectroscopic data and the insolubility of the product give further support for this conclusion.

Raman spectra were recorded for both the orange powder and the red crystals that were used for the X-ray structure determination. The adduct $TeCl_4{\cdot}S_4N_4$ belongs to the point group C_s and, therefore, all 33 fundamental vibrations are Raman active. The observed and calculated B3PW91/(RLC ECP) fundamental vibrations together with the main contributions to their potential energy distributions are given in Table 1, and the observed and calculated spectra are shown in Figure 1. The calculated values yield a good agreement with the observed wavenumbers and Raman activities (the DFT calculations are discussed in more detail below).[21] The four observed Raman lines in the region 672–1045 cm^{-1} are mainly due to ν_{S-N} stretching modes. The ν_{Te-Cl} stretching is the main contributor to the line at 265 cm^{-1} and also appears to be the major vibrational mode of the strongest Raman line at 296 cm^{-1} together with a torsion mode. The remainder of the Raman lines are predominantly torsional vibrations with the exception of the lines at 138 and 149 cm^{-1} for which the δ_{ClTeCl} bending mode is also a significant contributor.

Crystal Structure of $TeCl_4{\cdot}S_4N_4$ (1)

The crystal structure of $TeCl_4{\cdot}S_4N_4$ (**1**) with the atomic numbering scheme is shown in Figure 2(d), and the selected bond parameters are compared with those for related S_4N_4 adducts in Table 2. The molecule consists of an opened mo-

Table 1. Observed Raman and IR spectra, and calculated B3PW91/(RLC ECP) Fundamental vibrations [cm^{-1}], Raman intensities, and IR intensities of $TeCl_4{\cdot}S_4N_4$ (C_s).

Calcd.[a]		Raman obsd.	$I_{obsd.}$	$I_{calcd.}$[c]	IR[b]	$I_{obsd.}$	$I_{calcd.}$[c]	Potential energy distribution [%][d]
					1156	vw		
1072	a′′			6	1048	vs	90	78 ν_{NS}
1043	a′	1045	10	38			2	64 ν_{NS}, 18 τ, 10 δ_{NSN}
973	a′′			5	966	vs	30	75 ν_{NS}, 12 δ_{NSN}
833	a′′	807	1	6	807	s	36	50 ν_{NS}, 20 τ, 14 δ_{TeNS}, 12 δ_{ClTeN}
758	a′	761	42	79	760	vs	35	34 ν_{NS}, 21 τ, 14 ν_{TeN}, 13 δ_{SNS}
					727	w		
681	a′	672	2	2	671	m	8	44 ν_{NS}, 23 τ, 16 δ_{SNS}
634	a′′			4	635	m	22	46 ν_{NS}, 41 τ, 10 δ_{SNS}
616	a′	611	19	45	613	m, sh	<1	52 τ, 17 ν_{NS}, 16 δ_{NSN}
559	a′	566	9	23	563	w	6	27 τ, 25 ν_{NS}, 18 δ_{SNS}, 17 δ_{NSN}
					549	w		
521	a′′			2	500	s, br	44	30 δ_{NSN}, 29 τ, 24 δ_{SNS}, 12 ν_{NS}
411	a′	415	11	25			27	57 τ, 15 δ_{NSN}
364	a′′			<1	360	vs, br	19	81 τ
342	a′	350	30	45			18	79 τ
296	a′	296	100	100			13	40 τ, 39 ν_{TeCl}
282	a′′			7	251	s, br	100	47 ν_{TeCl}, 38 τ
281	a′			8			96	54 ν_{TeCl}, 30 τ
257	a′′	265	61	45			1	76 ν_{TeCl}
250	a′			7			11	76 τ
247	a′′	248	39	6			<1	43 τ, 17 δ_{NSN}, 11 δ_{TeNS}, 10 δ_{ClTeN}
231	a′			12			<1	69 τ
211	a′	212	33	10	225	w	1	70 τ, 11 δ_{SNS}
173	a′′	175	39	20			1	48 τ, 15 δ_{NSN}, 11 δ_{TeNS}
155	a′	169	54	12			8	25 τ, 13 δ_{SNS}, 12 δ_{ClTeCl}, 12 ν_{TeN}, 10 δ_{ClTeN}
143	a′	149	54	9			20	37 τ, 29 δ_{ClTeCl}, 19 δ_{ClTeN}
132	a′	138	61	10			<1	43 τ, 41 δ_{ClTeCl}
118	a′′			1			<1	63 τ, 17 δ_{ClTeC}
112	a′	109	22	2			1	64 τ, 14 δ_{ClTeCl}
99	a′′	102	21	1			<1	43 τ, 23 δ_{ClTeCl}, 22 δ_{ClTeN}
87	a′′	91	30	2			<1	43 τ, 15 δ_{ClTeN}, 13 ν_{TeCl}, 11 δ_{ClTeCl}
86	a′			6			1	43 τ, 14 δ_{ClTeN}, 11 δ_{ClTeCl}, 11 ν_{TeCl}, 10 δ_{SNS}
79	a′′	76	7	3			<1	77 τ
67	a′						<1	79 τ
26	a′′						<1	90 τ

[a] The calculated wavenumbers have been scaled by the factor of 0.993 to eliminate systematic errors.[55] [b] Ref.[15] [c] B3PW91/(RLC ECP) Raman activities. [d] The assignment is based on the most significant contributions (>10%) in the potential energy distribution.

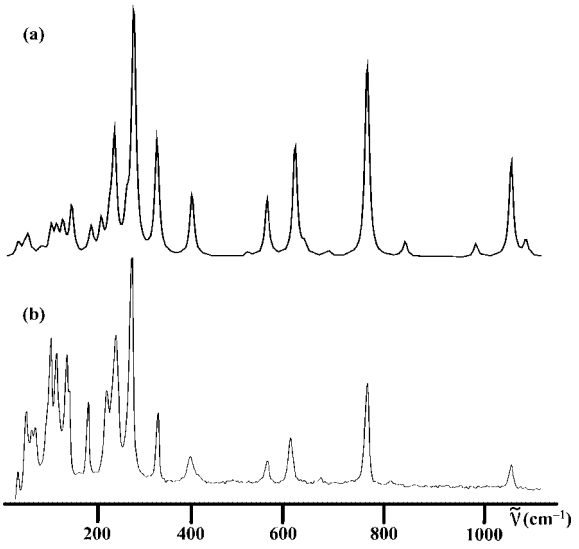

Figure 1. (a) Calculated B3PW91/(RLC ECP) fundamental vibrations and Raman activities of $TeCl_4{\cdot}S_4N_4$ (**1**). (b) Observed Raman spectrum of $TeCl_4{\cdot}S_4N_4$ (**1**).

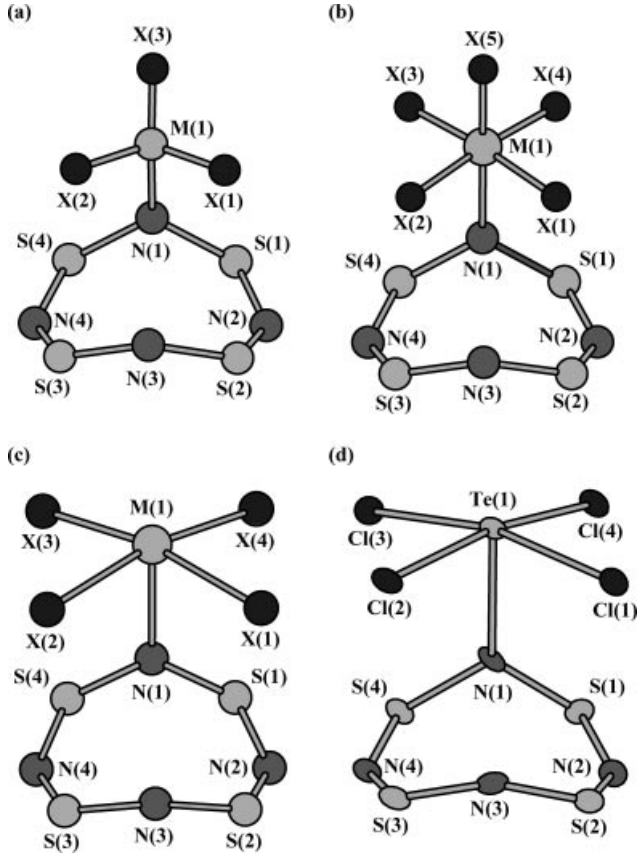

Figure 2. The B3PW91/(RLC ECP)-optimized geometries of (a) $BF_3{\cdot}S_4N_4$ (**2**) and $SO_3{\cdot}S_4N_4$ (**4**), (b) $AsF_5{\cdot}S_4N_4$ (**4**) and $SbCl_5{\cdot}S_4N_4$ (**6**), (c) $TeX_4{\cdot}S_4N_4$ [X = F (**6**), Cl (**1**), Br (**7**)] and $SeX_4{\cdot}S_4N_4$ [X = F (**8**), Cl (**9**), Br (**10**)]. (d) The X-ray structure of $TeCl_4{\cdot}S_4N_4$ (**1**). The thermal ellipsoids have been drawn at 50% probability level. The numbering of the atoms in all adducts is indicated in the figures.

nocyclic S_4N_4 ring in boat conformation that is bonded to $TeCl_4$ through one nitrogen atom. The S–N bond lengths [range 1.55(1)–1.67(1) Å] and the S–N–S bond angles (range 110.2–140.7°) in **1** are in good agreement with those reported for other adducts of S_4N_4 (Table 2).[1–9] The S(2)–S(4) and S(1)–S(3) distances [4.09(1) and 4.125(1) Å] across the ring are significantly longer than the corresponding distances in S_4N_4 [2.595(1) and 2.590(1) Å][26] indicating the expected loss of transannular S···S interaction.

The Te–N bond length of 2.16(1) Å in $TeCl_4{\cdot}S_4N_4$ is significantly longer than the single bond length[27] and ca. 0.12 Å longer than the Cl_4Te–N bond length in $[Te_6N_8(TeCl_4)_4]{\cdot}4THF$.[12] The Te–Cl bonds [2.464(3)–2.504(4) Å] are similar to the bond length of 2.516(4) Å in $[Te_6N_8(TeCl_4)_4]{\cdot}4THF$.[13] The shortest intermolecular Te···Cl contacts in $TeCl_4{\cdot}S_4N_4$ are 3.37(1) and 3.44(2) Å and are typical for secondary bonding interactions involving tellurium {for instance, the shortest intermolecular Te···Cl contact in $[Cl_2Te(\mu\text{-}NtBu)_2TeCl_2]_3$ is 3.107(1) Å[30]}. These contacts and a weak intermolecular S···N interaction link the molecules into a three-dimensional network (see Figure 3).

A DFT Study of Selected Lewis Acid Adducts of S_4N_4

The B3PW91/(RLC ECP)-optimized geometries of $TeCl_4{\cdot}S_4N_4$, $BF_3{\cdot}S_4N_4$, $SO_3{\cdot}S_4N_4$, $AsF_5{\cdot}S_4N_4$, $SbCl_5{\cdot}S_4N_4$, and $S_4N_4H^+$ are shown in Table 2 and compared to experimental information from crystal structure determinations. Whereas the optimized bond lengths show a slight overestimation, it can be seen that the calculated bond angles are close to the experimental values. The RMS deviation between the calculated and observed bond lengths is only 0.034 Å and that of the bond angles is 2°. The optimized geometries of all adducts exhibit local minima with molecular symmetry C_s. The geometries are slightly distorted from the ideal in the crystal structures due to packing effects in the lattices. The optimized bond parameters of $TeF_4{\cdot}S_4N_4$, $TeBr_4{\cdot}S_4N_4$, and $SeX_4{\cdot}S_4N_4$ (X = F, Cl, Br) are shown in Table 3 and exhibit features similar to those species for which experimental information is available (c.f. Table 2).

The S_4N_4 ring in all adducts shows similar structural features irrespective of the identity of the Lewis acid (see Figure 2). The transannular S···S interactions of the free S_4N_4 cage are absent and, in each adduct, the molecule exhibits a monocyclic ring in the boat conformation.[31]

The B3PW91/(RLC ECP) natural atomic charges and Mayer–Mulliken bond orders of the adducts **1**–**10** are shown in Table 4. With the exception of values involving N(1), the atomic charges and bond orders within the S_4N_4 ring are virtually independent of the Lewis acid. While the bond orders of N(1)–S(1) and N(1)–S(4) bonds are close to unity, those of other S–N bonds are significantly higher. This might indicate delocalization of π-electron density, but the high bond orders and consequently short S–N bond lengths have also been discussed in terms of electrostatic reinforcement of the bonds.[32–36]

The bond orders of the M(1)–N(1) bond and the natural atomic charges of M(1) and N(1) expectedly show variation

Table 2. Selected bond lengths [Å] and angles [°] of $TeCl_4{\cdot}S_4N_4$, $BF_3{\cdot}S_4N_4$, $SO_3{\cdot}S_4N_4$, $AsF_5{\cdot}S_4N_4$, $SbCl_5{\cdot}S_4N_4$, and $S_4N_4H^+$.

	$TeCl_4{\cdot}S_4N_4$		$BF_3{\cdot}S_4N_4$		$SO_3{\cdot}S_4N_4$		$AsF_5{\cdot}S_4N_4$		$SbCl_5{\cdot}S_4N_4$		$S_4N_4H^+$	
	Expt.[a]	DFT[b]	Expt.[c]	DFT[b]	Expt.[d]	DFT[b]	Expt.[e]	DFT[b]	Expt.[f]	DFT[b]	Expt.[g]	DFT[b]
S(1)–N(1)	1.63(1)	1.672	1.666(5)	1.667	1.668(4)	1.669	1.64(1)	1.668	1.662(9)	1.667	1.656(3)	1.688
S(1)–N(2)	1.59(1)	1.608	1.595(5)	1.615	1.575(6)	1.613	1.60(2)	1.612	1.581(9)	1.610	1.582(2)	1.607
S(2)–N(2)	1.55(1)	1.570	1.542(6)	1.569	1.555(6)	1.566	1.56(2)	1.567	1.53(1)	1.570	1.573(2)	1.561
S(2)–N(3)	1.60(1)	1.599	1.580(6)	1.604	1.585(6)	1.602	1.59(2)	1.601	1.59(1)	1.602	1.555(2)	1.603
S(3)–N(3)	1.57(1)	1.599	1.588(6)	1.604	1.593(5)	1.602	1.57(2)	1.601	1.58(1)	1.602	1.569(2)	1.603
S(3)–N(4)	1.56(1)	1.570	1.550(6)	1.569	1.511(7)	1.566	1.55(2)	1.567	1.54(1)	1.570	1.539(3)	1.561
S(4)–N(4)	1.59(1)	1.608	1.591(6)	1.615	1.616(6)	1.613	1.58(2)	1.612	1.57(1)	1.610	1.595(3)	1.607
S(4)–N(1)	1.67(1)	1.672	1.651(5)	1.667	1.688(4)	1.699	1.70(1)	1.668	1.651(9)	1.667	1.643(3)	1.688
M(1)–N(1)	2.16(1)	2.174	1.577(8)	1.632	1.749(4)	1.935	1.90(1)	1.992	2.134(7)	2.249	0.72(3)	1.019
M(1)–X(1)	2.448(3)	2.503	1.371(8)	1.381	1.429(6)	1.463	1.71(1)	1.752	2.352(4)	2.416		
M(1)–X(2)	2.504(4)	2.503	1.371(7)	1.381	1.428(5)	1.463	1.72(1)	1.752	2.360(3)	2.416		
M(1)–X(3)	2.501(3)	2.500	1.377(8)	1.365	1.442(5)	1.453	1.72(1)	1.737	2.342(3)	2.408		
M(1)–X(4)	2.464(3)	2.500					1.73(1)	1.737	2.359(3)	2.408		
M(1)–X(5)							1.70(1)	1.709	2.334(3)	2.363		
N(1)–S(1)–N(2)	110.2(6)	109.7	110.3(3)	110.9	108.6(3)	111.4	110.5(8)	111.0	110.1(5)	110.3	109.7(1)	110.9
S(1)–N(2)–S(2)	141(1)	137.4	137.6(4)	136.4	139.0(4)	137.2	137(1)	137.8	138.4(8)	137.2	138.9(2)	141.4
N(2)–S(2)–N(3)	119.2(7)	121.4	120.2(3)	121.5	119.7(3)	121.4	119.1(8)	121.6	120.8(6)	121.6	119.3(1)	119.7
S(2)–N(3)–S(3)	139.0(9)	139.2	137.9(4)	136.9	140.0(4)	137.9	139(1)	138.4	138.4(8)	138.0	138.1(1)	137.1
N(3)–S(3)–N(4)	118.9(7)	121.4	121.3(3)	121.5	121.2(3)	121.4	118.4(9)	121.6	119.6(6)	121.6	118.8(1)	119.7
S(3)–N(4)–S(4)	140.5(9)	137.4	137.3(4)	136.4	137.7(3)	137.2	140(1)	137.8	139.7(8)	137.2	138.0(2)	141.4
N(4)–S(4)–N(1)	110.7(6)	109.7	110.2(3)	110.9	107.6(3)	111.4	109.1(8)	111.0	109.8(5)	110.3	111.1(1)	110.9
S(4)–N(1)–S(1)	112.6(6)	112.7	112.7(3)	111.7	116.3(3)	114.7	112.3(8)	113.6	112.6(5)	112.0	118.4(1)	119.5
S(1)–N(1)–M(1)	123.9(6)	122.3	121.1(4)	123.1	124.5(3)	121.5	124.7(8)	123.1	123.3(5)	123.2	113(2)	118.8
S(4)–N(1)–M(1)	123.0(7)	122.3	126.0(4)	123.1	119.2(3)	121.5	123.1(7)	123.1	123.4(5)	123.2	121(2)	118.8
N(1)–M(1)–X(1)	84.6(3)	84.5	107.1(5)	104.7	101.1(3)	98.0	88.2(6)	87.0	89.2(2)	86.1		
N(1)–M(1)–X(2)	82.1(3)	84.5	109.2(5)	104.7	103.8(2)	98.0	89.8(6)	87.0	88.1(3)	86.2		
N(1)–M(1)–X(3)	81.7(3)	82.7	108.9(5)	107.4	104.4(3)	101.4	90.3(6)	86.6	88.0(2)	85.3		
N(1)–M(1)–X(4)	86.7(3)	82.7					89.1(6)	86.6	88.5(3)	85.3		
N(1)–M(1)–X(5)							178.5(6)	179.7	179.8(2)	180.0		
X(1)–M(1)–X(2)	91.5(1)	90.2	111.1(5)	113.0	115.0(3)	117.4	90.2(6)	89.4	90.6(1)	90.1		
X(1)–M(1)–X(3)	166.3(1)	167.2	112.2(5)	113.0	116.9(4)	117.6	178.5(6)	173.6	177.2(1)	171.5		
X(1)–M(1)–X(4)	89.9(1)	88.6					89.9(6)	89.4	88.8(1)	89.3		
X(1)–M(1)–X(5)							91.3(6)	92.7	90.9(1)	93.8		
X(2)–M(1)–X(3)	87.3(1)	88.6	108.3(5)	113.1	113.2(3)	117.6	89.8(6)	89.3	89.8(1)	89.3		
X(2)–M(1)–X(4)	168.5(1)	167.2					178.9(6)	173.6	176.5(1)	171.5		
X(2)–M(1)–X(5)							91.5(6)	92.7	91.7(1)	93.9		
X(3)–M(1)–X(4)	88.7(1)	89.7					90.1(6)	91.2	90.7(1)	89.9		
X(3)–M(1)–X(5)							90.2(6)	93.6	91.9(1)	94.7		
X(4)–M(1)–X(5)							89.6(6)	93.6	91.7(1)	94.7		

[a] This work. [b] The calculations have been carried out at the B3PW91/(RLC ECP) level of theory. [c] Ref.[1] [d] Ref.[2] [e] Ref.[3] [f] Ref.[6] [g] Ref.[19]

with respect to the identity of MX_n, and therefore play a role in the stabilities of the adducts.

The calculated energies of formation of the different Lewis acid adducts of S_4N_4 are listed in Table 5 (see Supporting Information for zero-point energy-corrected total energies of the relevant molecular species). While the formation of each adduct is an energetically favorable process, the energy changes span a wide range of values from almost energy-neutral formation of $SeBr_4{\cdot}S_4N_4$ to a very strongly exothermic reaction yielding $AsF_5{\cdot}S_4N_4$. There are two qualitative trends that affect the energy of formation, as shown in Figure 4. On one hand, the energy of formation becomes less negative with increasing M(1)–N(1) bond order. On the other hand, the energy of formation becomes more negative with increasing difference of charges between the M(1) and N(1) atoms. It can be concluded that the most stable adducts have the largest ionic contribution and the smallest covalent contribution in their M(1)–N(1) bonds.

Vibrational Spectroscopy

As discussed above, the calculated fundamental vibrations and Raman activities of $TeCl_4{\cdot}S_4N_4$ yield a good agreement with the observed Raman spectrum and provide the definite identification of the orange bulk powder that is obtained from the direct reaction of S_4N_4 and $TeCl_4$ (see Table 1). The Raman spectrum of the red crystals that were obtained as a side product in the reaction of $(Me_3SiNSN)_2S$ and $TeCl_4$ was virtually identical with that recorded for the orange powder.

The observed IR spectra of $BF_3{\cdot}S_4N_4$,[37] $SO_3{\cdot}S_4N_4$,[2] $AsF_5{\cdot}S_4N_4$,[38] $SbCl_5{\cdot}S_4N_4$,[15] $SeCl_4{\cdot}S_4N_4$,[15] and $TeF_4{\cdot}S_4N_4$[15] are also in good agreement with the calculated B3PW91/(RLC ECP) wavenumbers and intensities, as shown in the Supporting Information. This good agreement between the calculated and observed parameters also enables the prediction of both IR and Raman spectra of

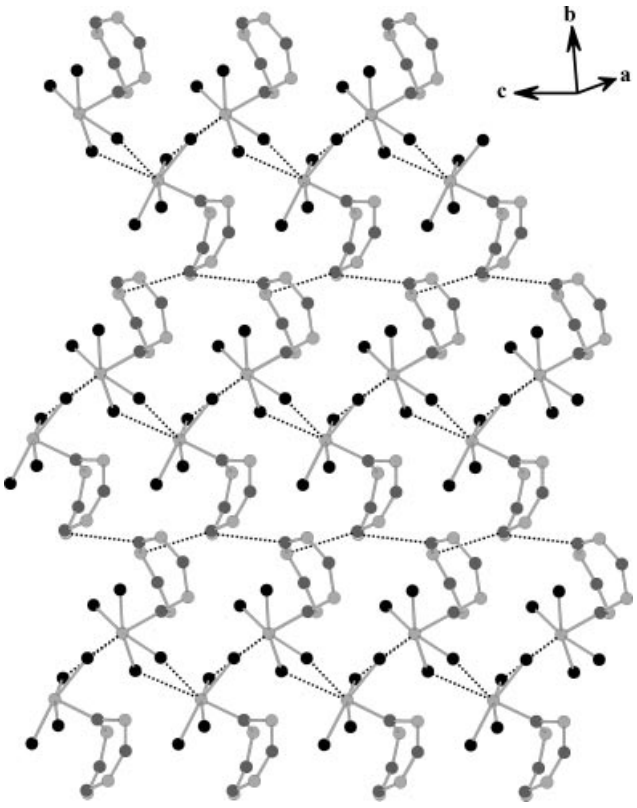

Figure 3. The closest Te···Cl contacts of 3.37(1) and 3.44(2) Å and the closest S···N contact of 3.31(1) Å link the $TeCl_4{\cdot}S_4N_4$ molcules into a continuous network.

Table 3. The B3PW91/(RLC ECP)-optimized bond lengths [Å] and angles [°] of $TeF_4{\cdot}S_4N_4$ (**6**), $TeBr_4{\cdot}S_4N_4$ (**7**), and $SeX_4{\cdot}S_4N_4$ [X = F (**8**), Cl (**9**), Br (**10**)].

	$TeF_4{\cdot}S_4N_4$	$TeBr_4{\cdot}S_4N_4$	$SeF_4{\cdot}S_4N_4$	$SeCl_4{\cdot}S_4N_4$	$SeBr_4{\cdot}S_4N_4$
S(1)–N(1)	1.665	1.672	1.659	1.663	1.670
S(1)–N(2)	1.612	1.610	1.611	1.609	1.610
S(2)–N(2)	1.568	1.571	1.567	1.570	1.571
S(2)–N(3)	1.601	1.599	1.598	1.597	1.597
S(3)–N(3)	1.601	1.599	1.598	1.597	1.597
S(3)–N(4)	1.568	1.571	1.567	1.570	1.571
S(4)–N(4)	1.612	1.610	1.611	1.609	1.610
S(4)–N(1)	1.665	1.672	1.659	1.663	1.670
M(1)–N(1)	2.156	2.205	1.993	2.022	2.018
M(1)–X(1)	1.978	2.672	1.869	2.375	2.547
M(1)–X(2)	1.978	2.672	1.869	2.375	2.547
M(1)–X(3)	1.960	2.675	1.841	2.375	2.557
M(1)–X(4)	1.960	2.675	1.841	2.375	2.557
N(1)–S(1)–N(2)	110.6	109.8	110.9	109.7	109.5
S(1)–N(2)–S(2)	137.1	137.2	137.2	137.1	137.2
N(2)–S(2)–N(3)	121.7	121.6	121.8	121.7	121.5
S(2)–N(3)–S(3)	138.5	139.3	139.7	140.5	140.6
N(3)–S(3)–N(4)	121.7	121.6	121.8	121.7	121.5
S(3)–N(4)–S(4)	137.1	137.2	137.2	137.1	137.2
N(4)–S(4)–N(1)	110.6	109.8	110.9	109.7	109.5
S(4)–N(1)–S(1)	113.5	112.5	116.0	115.4	114.4
S(1)–N(1)–M(1)	123.2	122.2	122.0	121.2	121.3
S(4)–N(1)–M(1)	123.2	122.2	122.0	121.2	121.3
N(1)–M(1)–X(1)	78.6	86.0	81.9	88.2	90.4
N(1)–M(1)–X(2)	78.6	86.0	81.9	88.2	90.4
N(1)–M(1)–X(3)	77.8	83.5	81.0	85.5	87.2
N(1)–M(1)–X(4)	77.8	83.5	81.0	85.5	87.2
X(1)–M(1)–X(2)	87.8	90.4	89.1	90.5	90.7
X(1)–M(1)–X(3)	156.4	169.5	163.0	173.7	177.6
X(1)–M(1)–X(4)	86.5	89.9	87.8	89.3	89.6
X(2)–M(1)–X(3)	86.5	89.9	87.8	89.3	89.6
X(2)–M(1)–X(4)	156.4	169.5	163.0	173.7	177.6
X(3)–M(1)–X(4)	89.6	89.7	90.3	90.5	90.0

$SeF_4{\cdot}S_4N_4$, $SeBr_4{\cdot}S_4N_4$, and $TeBr_4{\cdot}S_4N_4$ for which no experimental information is available (see Supporting Information).

Conclusions

The X-ray structure of $TeCl_4{\cdot}S_4N_4$ reveals features similar to those reported for other 1:1 adducts of S_4N_4 with Lewis acids. The coordination of a nitrogen centre to the acid results in loss of the transannular S···S interactions in S_4N_4 ring, which adopts a boat conformation. DFT calculations for a series of 1:1 adducts reveal that the π electron density in the ring is delocalized. Consequently, all S–N bond lengths lie between those of single and double bonds. The B3PW91/(RLC ECP) Mayer–Mulliken bond orders support this conclusion. The bond parameters, natural atomic charges, and bond orders within the S_4N_4 ring are rather insensitive to the chemical identity of the Lewis acid, the most notable exceptions being the charge on the nitrogen atom that is bonded to the acid molecule.

The B3PW91/(RLC ECP) energies of formation of the adducts from their component molecules vary significantly. The formation of $AsF_5{\cdot}S_4N_4$ is most exothermic and that of $SeBr_4{\cdot}S_4N_4$ is almost thermoneutral. The DFT calculations qualitatively show that the relative stabilities of the adducts with respect to their components depend on the ionic character of the M–N bond.

The fundamental vibrations calculated at the B3PW91/(RLC ECP) level of theory show good agreement with the experimental IR and Raman vibrations and their intensities. The calculations indicate that vibrational spectroscopy can be used to identify the species formed upon adduct formation and that this level of theory is sufficient to predict the vibrational spectra of the adducts that are still unknown.

Experimental Section

General Procedures: All reactions and manipulations of air- and moisture-sensitive reagents were carried out under argon passed through P_4O_{10}. The reagents SCl_2, SO_2Cl_2 and $TeCl_4$ (Aldrich) were used without further purification. $[(Me_3Si)_2N]_2S$ was prepared from $(Me_3Si)_2NH$ by utilizing the method of Wolmershäuser et al.[39] and purified by distillation. S_4N_4 was produced by the reaction of $[(Me_3Si)_2N]_2S$ with a mixture of SCl_2 and SO_2Cl_2.[40] Dichloromethane was dried by distillation over P_4O_{10} under nitrogen prior to use.

Spectroscopic Methods and Vibrational Analysis: The ^{14}N and ^{125}Te NMR spectra were recorded in dichloromethane with a Bruker DPX 400 spectrometer operating at 28.909 and 126.240 MHz, respectively. The spectral widths were 14.49 and 95.24 kHz, yielding

Table 4. B3PW91/(RLC ECP) natural atomic charges and Mayer–Mulliken bond orders in **1**–**10**.

	$MX_3{\cdot}S_4N_4$[a]		$MX_5{\cdot}S_4N_4$[b]			$MX_4{\cdot}S_4N_4$[c]					$S_4N_4H^+$
	2	**3**	**4**	**5**	**6**	**1**	**7**	**8**	**9**	**10**	**11**
Natural atomic charges											
S(1)	1.02	1.03	1.05	1.06	1.05	1.06	1.05	1.06	1.08	1.08	1.03
N(1)	–1.17	–1.20	–1.26	–1.20	–1.26	–1.24	–1.23	–1.20	–1.18	–1.17	–1.11
S(2)	1.21	1.23	1.23	1.22	1.23	1.23	1.22	1.25	1.24	1.23	1.30
N(2)	–0.96	–0.96	–0.96	–0.97	–0.96	–0.98	–0.98	–0.97	–0.98	–0.99	–0.95
S(3)	1.21	1.23	1.23	1.22	1.23	1.23	1.22	1.25	1.24	1.23	1.30
N(3)	–1.09	–1.10	–1.10	–1.09	–1.09	–1.08	–1.07	–1.07	–1.07	–1.07	–1.12
S(4)	1.02	1.03	1.06	1.06	1.05	1.06	1.05	1.06	1.08	1.08	1.30
N(4)	–0.96	–0.96	–0.96	–0.97	–0.96	–0.98	–0.98	–0.97	–0.98	–0.99	–0.95
M(1)	1.41	2.60	2.83	1.74	2.50	1.48	1.27	2.11	1.04	0.83	0.47
X(1)	–0.58	–0.99	–0.64	–0.42	–0.70	–0.47	–0.41	–0.65	–0.38	–0.33	
X(2)	–0.58	–0.99	–0.64	–0.42	–0.70	–0.47	–0.41	–0.65	–0.38	–0.33	
X(3)	–0.56	–0.94	–0.62	–0.40	–0.68	–0.43	–0.38	–0.62	–0.35	–0.30	
X(4)			–0.62	–0.40	–0.68	–0.43	–0.38	–0.62	–0.35	–0.30	
X(5)			–0.60	–0.36							
Mayer–Mulliken bond orders											
S(1)–N(1)	1.15	1.12	1.14	1.12	1.12	1.08	1.08	1.13	1.09	1.08	1.08
S(1)–N(2)	1.31	1.31	1.32	1.33	1.32	1.32	1.32	1.31	1.32	1.31	1.32
S(2)–N(2)	1.53	1.53	1.52	1.50	1.52	1.50	1.49	1.52	1.49	1.48	1.55
S(2)–N(3)	1.33	1.33	1.34	1.34	1.34	1.35	1.35	1.35	1.35	1.35	1.33
S(3)–N(3)	1.33	1.33	1.34	1.34	1.34	1.35	1.35	1.35	1.35	1.35	1.33
S(3)–N(4)	1.53	1.53	1.52	1.50	1.52	1.50	1.49	1.52	1.49	1.48	1.55
S(4)–N(4)	1.31	1.31	1.32	1.33	1.32	1.32	1.32	1.31	1.32	1.31	1.32
S(4)–N(1)	1.15	1.12	1.14	1.12	1.12	1.08	1.08	1.13	1.09	1.08	1.08
M(1)–N(1)	0.58	0.48	0.34	0.35	0.42	0.46	0.48	0.47	0.53	0.54	0.72
M(1)–X(1)	0.91	1.70	0.73	0.85	0.57	0.83	0.77	0.66	0.86	0.94	
M(1)–X(2)	0.91	1.70	0.73	0.85	0.57	0.83	0.77	0.66	0.86	0.94	
M(1)–X(3)	0.98	1.81	0.75	0.87	0.61	0.84	0.78	0.70	0.86	0.93	
M(1)–X(4)			0.75	0.87	0.61	0.84	0.78	0.70	0.86	0.93	
M(1)–X(5)			0.80	0.98							

[a] M = B, S; X = F, O. [b] M = As, Sb; X = F, Cl. [c] M = Te, Se; X = F, Cl, Br.

Table 5. B3PW91/(RLC ECP) energies of formation of $MX_n{\cdot}S_4N_4$.

Reaction			ΔE [kJ·mol^{-1}][a]
$BF_3 + S_4N_4$	→	$BF_3{\cdot}S_4N_4$	–81.4
$SO_3 + S_4N_4$	→	$SO_3{\cdot}S_4N_4$	–58.6
$SeF_4 + S_4N_4$	→	$SeF_4{\cdot}S_4N_4$	–42.2
$SeCl_4 + S_4N_4$	→	$SeCl_4{\cdot}S_4N_4$	–23.4
$SeBr_4 + S_4N_4$	→	$SeBr_4{\cdot}S_4N_4$	–8.2
$TeF_4 + S_4N_4$	→	$TeF_4{\cdot}S_4N_4$	–69.5
$TeCl_4 + S_4N_4$	→	$TeCl_4{\cdot}S_4N_4$	–43.0
$TeBr_4 + S_4N_4$	→	$TeBr_4{\cdot}S_4N_4$	–30.5
$AsF_5 + S_4N_4$	→	$AsF_5{\cdot}S_4N_4$	–116.3
$SbCl_5 + S_4N_4$	→	$SbCl_5{\cdot}S_4N_4$	–66.7

[a] The energy changes are based on total energies of the molecular species incorporating the zero-point-energy corrections.

the respective resolutions of 7.08 and 1.45 Hz/data point. The pulse widths were 12.0 μs for ^{14}N and 6.67 μs for ^{125}Te, corresponding to nuclear tip angles of 44 and 30°, respectively. All spectra were recorded unlocked. The ^{14}N NMR chemical shifts are reported relative to CH_3NO_2 and ^{125}Te NMR spectra were referenced externally to a saturated solution of H_6TeO_6. The MS-EI mass spectrum was recorded with a Micromass Quattro II spectrometer at 70 eV of electron energy. Raman spectra were recorded for solid samples at room temperature with a Bruker IFS-66 spectrometer equipped with a FRA-16 Raman unit and Nd:YAG laser (power 110 mW; 8–64 scans; spectral resolution ±1 cm^{-1}; Blackmann–Harris four-term apodization, no white light correction, 180 ° scattering geometry).

Preparation of $TeCl_4{\cdot}S_4N_4$ (1): S_4N_4 (0.092 g, 0.5 mmol) was dissolved in dichloromethane (10 mL) and added to a suspension of $TeCl_4$ (0.135 g, 0.5 mmol) in dichloromethane (10 mL) at –80 °C. The reaction mixture was stirred overnight and warmed slowly to room temperature to give a yellow solution and an orange, insoluble precipitate of **1** (0.174 g, 76%). This precipitate was used for vibrational and mass spectroscopic characterization of the product. The NMR spectrum was recorded from the yellow solution obtained after filtration. ^{14}N NMR (CH_2Cl_2, 25 °C): δ = –256 (S_4N_4) ppm. MS: *m*/*z* (%) = 46 (100) [SN^+], 78 (18) [S_2N^+], 92 (26) [$S_2N_2^+$], 130 (77) [Te^+], 138 (18) [$S_3N_3^+$], 144 (7) [TeN^+], 165 (72) [$TeCl^+$], 176 (25) [$TeSN^+$], 184 (5) [$S_4N_4^+$], 200 (52) [$TeCl_2^+$], 211 (22) [$TeClSN^+$], 235 (38) [$TeCl_3^+$], 246 (28) [$TeCl_2SN^+$], 257 (67) [$TeClS_2N_2^+$], 292 (19) [$TeCl_2S_2N_2^+$], 314 (5) [$TeS_4N_4^+$]. All fragments show expected isotopic distributions. The *m*/*z* and intensities in the list above refer to the fragments containing the ^{130}Te isotope.

X-ray Crystallography: A small number of red, moisture-sensitive crystals of $TeCl_4{\cdot}S_4N_4$ (**1**) were obtained by the reaction of $(Me_3SiNSN)_2S$ with $TeCl_4$ in CH_2Cl_2.[41] *FW* = 453.68 g/mol, monoclinic, space group *Cc*, *a* = 12.998(2), *b* = 11.914(2), *c* = 7.214(1) Å, β = 101.65(1)°; *V* = 1080.5(3) Å^3; *Z* = 4, D_c = 2.789 g cm^{-3}; *F*(000) = 848; μ(Mo-K_α) = 4.471 mm^{-1}, *T* = 120 K, crystal dimensions 0.2 × 0.1 × 0.1 mm^3. Reflections (2890 total, 1610 unique, θ range 3.42–26.00°, R_{int} = 0.0369) were collected on Nonius Kappa CCD diffractometer using graphite-monochromated Mo-K_α radiation (λ = 0.71073 Å). The intensity data were corrected for Lorentz and polarization effects, and an empirical absorption correction was applied to the net intensities. The structure was solved by direct meth-

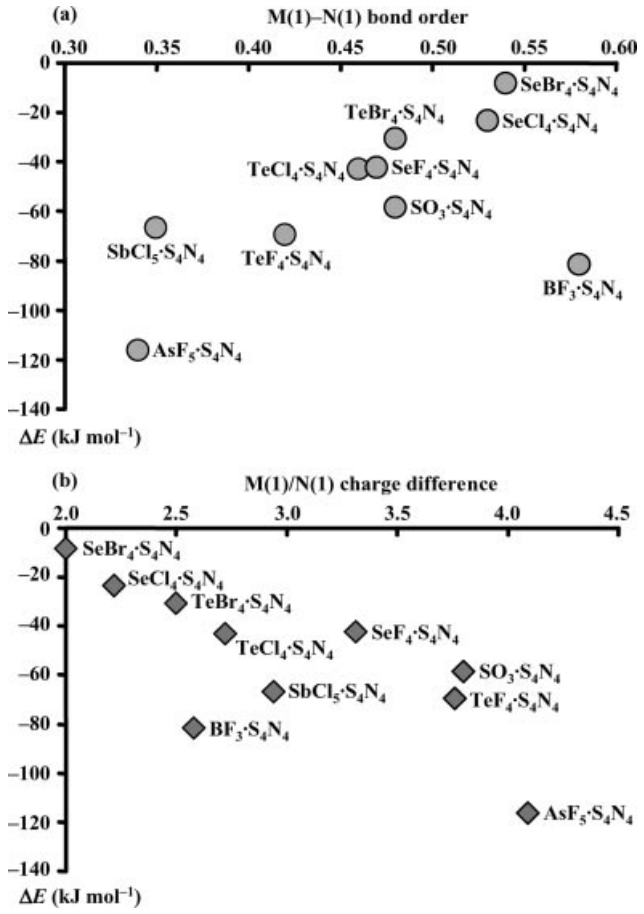

Figure 4. The dependence of the B3PW91/(RLC ECP) energy of formation of adducts **1**–**10** on (a) M(1)–N(1) bond order and (b) difference of atomic charges of M(1) and N(1) (see Table 4).

ods using SHELXS-97[43] and refined using SHELXL-97.[44] The scattering factors for the neutral atoms were those incorporated with the programs. The final $R_1 = 0.0515$ [$I > 2\sigma(I)$] and $wR_2 = 0.1242$ (all data) [$R_1 = \Sigma||F_o| - |F_c||/\Sigma|F_o|$, $wR_2 = [\Sigma w(F_o^2 - F_c^2)^2/\Sigma wF_o^4]1/2$, $w = [\sigma^2(F_o^2) + (0.0700P)^2 + 10.00P]^{-1}$ where $P = \{\max(F_o^2,0) + 2F_c^2\}/3$]. Maximum and minimum values in the final difference Fourier synthesis are 2.342 and –1.629 e·Å^{-3}.

Further details of the crystal-structure investigation of **1** can be obtained free of charge from the Fachinformationszentrum Karlsruhe, 76344 Eggenstein-Leopoldshafen, Germany, Fax: +49-7247-808-666, E-mail: crysdata@fiz-karlsruhe.de, http://www.fiz-karlsruhe.de (under "Products and Services") on quoting the depository number CSD-416253.

Computational Details: The molecular orbital calculations of $TeCl_4{\cdot}S_4N_4$ (**1**), $BF_3{\cdot}S_4N_4$ (**2**), $SO_3{\cdot}S_4N_4$ (**3**), $AsF_5{\cdot}S_4N_4$ (**4**), $SbCl_5{\cdot}S_4N_4$ (**5**), $TeF_4{\cdot}S_4N_4$ (**6**), $TeBr_4{\cdot}S_4N_4$ (**7**), and $SeX_4{\cdot}S_4N_4$ [X = F (**8**), Cl (**9**), Br (**10**)] were carried out at the DFT level of theory involving Becke's three parameter hybrid functionals with the Perdew/Wang 91 correlation (B3PW91)[45–51] and using the Stuttgart relativistic large core effective core potential approximation (RLC ECP)[52–54] by augmenting the double-zeta quality basis sets of the valence orbitals by two polarization functions for all atoms except for hydrogen for which a standard Pople-type 6-31G* basis was used, as implemented in Gaussian 98 and Gaussian 03. Complete geometry optimizations were performed for each adduct. Fundamental vibrations were calculated to establish the nature of the stationary points and to enable the assignment of the Raman spectra. The calculated wavenumbers and zero-point-energy corrections (ZPE) were scaled by 0.993 to eliminate the systematic errors.[55] The calculations were mainly performed with the GAUSSIAN 03 (Rev. B.04) program package.[56] The wavefunction files for NBO 5.0,[57] however, were calculated with the GAUSSIAN 98 (Rev. A.9) package.[58]

Supporting Information (see also the footnote on the first page of this article): Table S1. B3PW91/(RLC ECP) total and formation energies, and ZPE scaled by 0.993 of $MX_3(S_4N_4)$ (M = B, S; X = F, O), $MX_4(S_4N_4)$ (M = Se, Te; X = F, Cl, Br), $MX_5(S_4N_4)$ (M = As, Sb; X = F, Cl) and $S_4N_4H^+$. Table S2. Scaled B3PW91/(RLC ECP) fundamental vibrations of $MX_4(S_4N_4)$ (M = Se, Te; X = F, Cl, Br). Table S3. Scaled B3PW91/(RLC ECP) fundamental vibrations of $MX_3(S_4N_4)$ (M = B, S; X = F, O), $MX_5(S_4N_4)$ (M = As, Sb; X = F, Cl) and $S_4N_4H^+$.

Acknowledgments

Financial support from the Academy of Finland, the Emil Aaltonen Foundation, Finnish Cultural Foundation, and the Natural Sciences and Engineering Research Council (Canada) is gratefully acknowledged.

[1] M. G. B. Drew, D. H. Templeton, A. Zalkin, *Inorg. Chem.* **1967**, *6*, 1906.
[2] A. Gieren, B. Diederer, H. W. Roesky, N. Amin, O. Petersen, *Z. Anorg. Allg. Chem.* **1978**, *440*, 119.
[3] W. Isenberg, R. Mews, G. Sheldrick, *Z. Anorg. Allg. Chem.* **1985**, *525*, 54.
[4] D. Neubauer, J. Weiss, M. Becke-Goehring, *Z. Naturforsch. Teil B* **1959**, *14*, 284.
[5] D. Neubauer, J. Weiss, *Z. Anorg. Allg. Chem.* **1960**, *303*, 28.
[6] R. J. Gillespie, J. F. Sawyer, D. R. Slim, J. D. Tyrer, *Inorg. Chem.* **1982**, *21*, 1296.
[7] U. Thewalt, *Z. Anorg. Allg. Chem.* **1981**, *476*, 105.
[8] U. Thewalt, *Z. Naturforsch. Teil B* **1980**, *35*, 855.
[9] U. Thewalt, G. Albrecht, *Z. Naturforsch. Teil B* **1982**, *37*, 1098.
[10] U. Thewalt, K. Holl, *Z. Naturforsch. Teil B* **1988**, *43*, 467.
[11] H. Martan, J. Weiss, *Z. Anorg. Allg. Chem.* **1984**, *514*, 107.
[12] A. Gieren, K. Hofer, T. Hubner, *Z. Kristallogr.* **1987**, *178*, 68.
[13] W. Massa, C. Lau, M. Möhlen, B. Neumuller, K. Dehnicke, *Angew. Chem. Int. Ed. Engl.* **1998**, *37*, 2840.
[14] R. C. Paul, C. L. Arora, J. Kishore, K. C. Malhotra, *Aust. J. Chem.* **1971**, *24*, 1637.
[15] G. G. Alange, A. J. Banister, *J. Inorg. Nucl. Chem.* **1978**, *40*, 203.
[16] V. C. Ginn, P. F. Kelly, J. D. Woollins, *Polyhedron* **1994**, *13*, 1501.
[17] A. Haas, M. Pryka, *Chem. Ber.* **1995**, *128*, 11.
[18] A MNDO comparison of $S_4N_4H^+$ and some Lewis acid adducts of S_4N_4 has been presented by Cordes et al.[19]
[19] A. W. Cordes, C. G. Marcellus, M. C. Noble, R. T. Oakley, W. T. Pennington, *J. Am. Chem. Soc.* **1983**, *105*, 6008.
[20] T. Chivers, R. T. Oakley, O. J. Scherer, G. Wolmershäuser, *Inorg. Chem.* **1981**, *20*, 914.
[21] The assignment of the Raman spectra is also consistent with that which have recently been carried out for some related chalcogen-nitrogen systems.[22–25].
[22] A. Maaninen, J. Siivari, R. J. Suontamo, J. Konu, R. S. Laitinen, T. Chivers, *Inorg. Chem.* **1997**, *36*, 2170.
[23] A. Maaninen, R. S. Laitinen, T. Chivers, T. A. Pakkanen, *Inorg. Chem.* **1999**, *38*, 3450.
[24] A. Maaninen, J. Konu, R. S. Laitinen, T. Chivers, G. Schatte, J. Pietikäinen, M. Ahlgrén, *Inorg. Chem.* **2001**, *40*, 3559.
[25] R. Fleischer, B. Walfort, A. Gbureck, P. Scholz, W. Kiefer, D. Stalke, *Chem. Eur. J.* **1998**, *4*, 2266.

[26] M. L. DeLucia, P. Coppens, *Inorg. Chem.* **1978**, *17*, 2336.
[27] The sum of the covalent radii for tellurium and nitrogen is 2.07 Å.[28] The Te^{II}–N single bond lengths in $[(Me_3Si)_2N–Te–N(SiMe_3)_2]$ are 2.053(2) and 2.045(2) Å.[29]
[28] J. Emsley, *The Elements*, 3rd ed., Clarendon Press, Oxford **1998**.
[29] M. Björgvinsson, H. W. Roesky, F. Pauer, D. Stalke, G. M. Sheldrick, *Inorg. Chem.* **1990**, *29*, 5140.
[30] T. Chivers, N. Enright, N. Sandblom, G. Schatte, M. Parvez, *Inorg. Chem.* **1999**, *38*, 5431.
[31] The MNDO calculations of some Lewis acid adducts of S_4N_4 by Cordes et al.[19] lead to similar geometric and bonding features in the S_4N_4 ring as our present higher level DFT calculations.
[32] T.-H. Tang, R. F. W. Bader, P. J. MacDougall, *Inorg. Chem.* **1985**, *24*, 2047.
[33] W. Scherer, M. Spiegler, B. Pedersen, M. Tafipolsky, W. Hieringer, B. Reinhard, A. J. Downs, G. S. McGrady, *Chem. Commun.* **2000**, 635.
[34] D. Leusser, B. Walfort, D. Stalke, *Angew. Chem. Int. Ed.* **2002**, *41*, 2079.
[35] J. Henn, D. Hge, D. Leusser, D. Stalke, B. Engels, *J. Phys. Chem. B* **2004**, *108*, 9442.
[36] D. Leusser, J. Henn, N. Kocher, B. Engels, D. Stalke, *J. Am. Chem. Soc.* **2004**, *126*, 1781.
[37] K. J. Wynne, W. L. Jolly, *Inorg. Chem.* **1967**, *6*, 107.
[38] R. Mews, D.-L. Wagner, O. Glemser, *Z. Anorg. Allg. Chem.* **1975**, *412*, 148.
[39] G. Wolmershäuser, C. R. Brulet, G. B. Street, *Inorg. Chem.* **1978**, *17*, 3586.
[40] A. Maaninen, J. Siivari, R. S. Laitinen, T. Chivers, *Inorg. Synth.* **2003**, *3*, 196.
[41] We have recently observed that S_4N_4 is one product in the reaction of $(Me_3SiNSN)_2S$ with $TeCl_4$.[42] It reacts with unreacted $TeCl_4$ and forms a small amount of well-formed red crystals of $TeCl_4{\cdot}S_4N_4$ that were suitable for the X-ray structure determination. While the direct reaction between S_4N_4 and $TeCl_4$ yields an orange powder that could be shown by vibrational analysis and mass spectroscopy to be $TeCl_4{\cdot}S_4N_4$, we were unable to obtain single crystals from this direct reaction.
[42] J. Konu, M. Ahlgrén, S. M. Aucott, T. Chivers, S. H. Dale, M. R. J. Elsegood, K. E. Holmes, S. L. M. James, P. F. Kelly, R. S. Laitinen, *Inorg. Chem.* **2005**, *44*, 4992.
[43] G. M. Sheldrick, SHELXS-97, *Program for Crystal Structure Determination*, University of Göttingen, Göttingen, Germany, **1997**.
[44] G. M. Sheldrick, SHELXL-97, *Program for Crystal Structure Refinement*, University of Göttingen, Göttingen, Germany, **1997**.
[45] A. D. Becke, *J. Phys. Chem.* **1993**, *98*, 5648.
[46] K. Burke, J. P. Perdew, Y. Wang, *Electron Density Functional Theory: Recent Progress and New Directions* (Eds.: J. F. Dobson, G. Vignale, M. P. Das), Plenum, New York, **1998**.
[47] J. P. Perdew, *Electronic Structure of Solids* (Eds.: P. Ziesche, H. Eschrig), Akademie Verlag, Berlin, **1991**.
[48] J. P. Perdew, Y. Wang, *Phys. Rev. B* **1992**, *45*, 13244.
[49] J. P. Perdew, J. A. Chevary, S. H. Vosko, K. A. Jackson, M. R. Pederson, D. J. Singh, C. Fiolhais, *Phys. Rev. B* **1992**, *46*, 6671.
[50] J. P. Perdew, J. A. Chevary, S. H. Vosko, K. A. Jackson, M. R. Pederson, D. J. Singh, C. Fiolhais, *Phys. Rev. B* **1993**, *48*, 4978.
[51] J. P. Perdew, K. Burke, Y. Wang, *Phys. Rev. B* **1996**, *54*, 16553.
[52] W. Kuechle, M. Dolg, H. Stoll, H. Preuss, *Mol. Phys.* **1991**, *74*, 1245.
[53] A. Bergner, M. Dolg, W. Kuechle, H. Stoll, H. Preuss, *Mol. Phys.* **1993**, *80*, 1431.
[54] M. Buhl, W. Thiel, U. Fleischer, W. Kutzelnigg, *J. Phys. Chem.* **1995**, *99*, 4000.
[55] A. P. Scott, L. Radom, *J. Phys. Chem.* **1996**, *100*, 16502.
[56] M. J. Frisch, G. W. Trucks, H. B. Schlegel, G. E. Scuseria, M. A. Robb, J. R. Cheeseman, J. A. Montgomery Jr, T. Vreven, K. N. Kudin, J. C. Burant, J. M. Millam, S. S. Iyengar, J. Tomasi, V. Barone, B. Mennucci, M. Cossi, G. Scalmani, N. Rega, H. G. Petersson, A. Nakatsuji, M. Hada, M. Ehara, K. Toyota, R. Fukuda, J. Hasegawa, M. Ishida, T. Nakajima, Y. Honda, O. Kitao, H. Nakai, M.Klene, X. Li, J. E. Knox, H. P. B. Hratchian, J. Cross, C. Adamo, J. Jaramillo, R. Gomperts, R. E. Stratmann, O. Yazyev, A. J. Austin, R. Cammi, C. Pomelli, J. W. Ochterski, P. Y. Ayala, K. Morokuma, G. A. Voth, P. Salvador, J. J. Dannenberg, V. G. Zakrzewski, S. Dapprich, A. D. Daniels, M. C. Strain, O. Farkas, D. K. Malick, A. D. Rabuck, K. Raghavachari, J. B. Foresman, J. V. Ortiz, Q. Cui, A. G. Baboul, S. Clifford, J. Cioslowski, B. B. Stefanov, G. Liu, A. Liashenko, P. Piskorz, I. Komaromi, R. L. Martin, D. J. Fox, T. Keith, M. A. Al-Laham, C. Y. Peng, A. Nanayakkara, M. Challacombe, P. M. W. Gill, B. Johnson, W. Chen, M. W. Wong, C. Gonzalez, J. A. Pople, *Gaussian 03*, revision B.04, Inc., Pittsburgh PA, **2003**.
[57] E. D. Glendening, J. K. Badenhoop, A. E. Reed, J. E. Carpenter, J. A. Bohmann, C. M. Morales, F. Weinhold, *NBO 5.0*, Theoretical Chemistry Institute, University of Wisconsin, Madison, WI, **2001**.
[58] M. J. Frisch, G. W. Trucks, H. B. Schlegel, G. E. Scuseria, M. A. Robb, J. R. Cheeseman, V. G. Zakrzewski, J. A. Montgomery Jr, R. E. Stratmann, J. C. Burant, S. Dapprich, J. M. Millam, A. D. Daniels, K. N. Kudin, M. C. Strain, O. Farkas, J. Tomasi, V. Barone, M. Cossi, R. Cammi, B. Mennucci, C. Pomelli, C. Adamo, S. Clifford, J. Ochterski, G. A. Petersson, P. Y. Ayala, Q. Cui, K. Morokuma, D. K. Malick, A. D. Rabuck, K. Raghavachari, J. B. Foresman, J. Cioslowski, J. V. Ortiz, A. G. Baboul, B. B. Stefanov, G. Liu, A. Liashenko, P. Piskorz, I. Komaromi, R. Gomperts, R. L. Martin, D. J. Fox, T. Keith, M. A. Al-Laham, C. Y. Peng, A.Nanayakkara, M. Challacombe, P. M. W. Gill, B. Johnson, W. Chen, M. W. Wong, J. L. Andres, C. Gonzalez, M. Head-Gordon, E. S. Replogle, J. A. Pople, *Gaussian 98*, revision A.9, Inc., Pittsburgh PA, **1998**.

Received: February 17, 2006
Published Online: June 6, 2006

